International Journal of
INTELLIGENT SYSTEMS AND APPLICATIONS IN ENGINEERING
ISSN:2147-6799 www.ijisae.org Original Research Paper

Adaptive Backstepping Control of Renewable Energy Based Grid Interactive Charging Station for EV with Power Quality Improved

Boda Anusha[1], Md. Haseeb Khan[2], P. Satish Kumar[3]

Submitted: 14/05/2024 **Revised**: 27/06/2024 **Accepted**: 07/07/2024

Abstract: The Sophisticated control strategies for Grid Interactive Charging Stations (GICS) becomes imperative due to with the growing prominence of Electric Vehicles (EVs) and the increasing integration of renewable energy sources into power systems. This paper explores the application of Adaptive Backstepping Control in the context of a Renewable Energy-Based GICS for EVs, focusing on enhancing power quality during the charging process. The Adaptive Backstepping Control algorithm is designed to adapt to the dynamic and uncertain nature of renewable energy inputs, providing a robust and efficient control framework for the GICS. Through optimising power flow and regulating oscillations in renewable energy supply, the system aims to improve power quality metrics including voltage management and harmonic reduction during EV charging. The proposed control methodology is compared with an Adaptive Frequency-Fixed Second-Order Generalized Integrator featuring DC offset rejection capability. The comparison encompasses key performance indicators, including power quality indices, transient response, and overall system stability. The findings contribute to the advancement of control methodologies for GICS, ultimately fostering the development of sustainable and high-performance EV charging infrastructure integrated with renewable energy sources.

Keywords: *Grid Interactive Charging Station, Adaptive Backstepping Control, Renewable Energy Integration, Electric Vehicle Charging, Power Quality Improvement*

1. Introduction

The advent of Electric Vehicles (EVs) has catalysed a paradigm shift in the transportation sector, necessitating the development of robust charging infrastructure capable of accommodating the increasing demand for sustainable mobility [1-2]. Simultaneously, the integration of renewable energy sources into the power grid has become a focal point in addressing environment concerns and achieving energy sustainability. This article encapsulates the core theme of this study. At its essence, The study aims to solve the issues connected with the dynamic and intermittent nature of renewable energy sources in the context of Grid Interactive Charging Stations (GICS) for Electric Vehicles. Additionally, the focus extends to enhancing power quality during the charging process, recognizing the pivotal role that stable and reliable power systems play in the successful integration of EVs into mainstream transportation [3].The rise of EVs has brought about a significant change in transportation, requiring the creation of sturdy charging systems to meet the growing need for sustainable mobility [4].This convergence of EV technology and renewable energy systems has given rise to innovative solutions, and the research presented herein aims to contribute to this evolving landscape [5]. Meeting the escalating demand for EV charging necessitates the establishment of a substantial charging infrastructure, predominantly reliant on support from the grid [6]. Consequently, the imperative arises to design a charging system that not only caters to the burgeoning EV charging demand but also concurrently addresses and expands the power feature of the grid [7]. The deployment of Renewable Energy-Based GICS introduces a compelling synergy between sustainable energy generation and electric vehicle charging infrastructure. Harnessing the power of wind, solar, or other renewable sources for EV charging not only reduces the carbon footprint associated with transportation but also aligns with global initiatives aimed at transitioning towards cleaner and greener energy ecosystems [8]. In this pursuit, the research employs an Adaptive Backstepping Control algorithm, a sophisticated control strategy well-suited for systems characterized by dynamic and uncertain behavior. The Adaptive Backstepping Control provides a means to navigate the complexities of renewable energy integration into the power grid, ensuring stability, efficiency, and improved power quality during EV charging operations [9].

Meeting the escalating demand for Electric Vehicle (EV) charging necessitates the establishment of a substantial charging infrastructure, predominantly reliant on support from the grid [10]. Designing a charging infrastructure that simultaneously solves and enhances the grid's power quality and meets the growing demand for EV charging is therefore essential [11]. Two prominent theories among these are the Synchronous Reference Frame Theory (SRFT) [13] and the

[1] *Reseach Schola in Drepartment of Electrical Engineering, University College of Engineering, Osmania University, Hyderabad, India. bodanusha@gmail.com*
[2] *Professor & Head of the Department of Electrical Engineering , Muffa Kham Jah College of Engineering & Technology, Hyderabad, India. haseebkhaneed@mjcollege.ac.in*
[3] *Professor in the Department of electrical engineering, University College of engineering, Osmania University, Hyderabad, India. satish_8020@yahoo.co.in*

Instantaneous Reactive Power Theory (IRPT) [12]. Enhanced PLL (EPLL) is an other strategy that shows excellent tracking efficiency in these circumstances [14–15]. At the other extreme, the approach based on the Second Order Generalised Integrator (SOGI) [16] shows promising tracking properties together with quick convergence and minimal steady-state error.

Notch Filters (NFs) [17] provide performance like SOGI algorithms, but selecting the centre frequency at variable frequencies proves challenging, impacting NF performance. Attempts have been made to address this limitation with adaptive notch filters (ANF) [18], permitting the centre frequency to adjust in response to variations in the signal frequency. Nevertheless, the frequency feedback loop limits ANF's functionality. The frequency feedback problem is solved by the SOGI-Frequency Locked Loop (SOGI-FLL) [19], which performs better than SOGI and other algorithms. Frequency-Fixed SOGI (FF-SOGI) was developed as a result of efforts to break the frequency feedback loop and improve performance [20–22]. To account for this, it is recommended in [23] that the quadrature signal be increased by a gain equal to the ratio of frequency drift and the nominal frequency. Regretfully, while employing SRF-PLL for frequency estimation, the FF-SOGI method becomes computationally costly. The Adaptive FF-SOGI (AFF-SOGI) approach was introduced [24] as a solution to this problem.

The Adaptive Backstepping algorithm, as adopted in this research, offers distinct advantages. It demonstrates adaptability in dynamically responding to variations in grid conditions, making it well-suited for mitigating challenges associated with distorted and unbalanced voltages. The integration of dc offset rejection capability further enhances its robustness, addressing a critical aspect of power quality in the context of EV charging. By leveraging these attributes, the proposed stands out as a promising solution for simultaneously managing EV charging and augmenting grid power quality.

In order to improve grid power quality, this paper examines a multifunctional charging station that combines a photovoltaic (PV) array and a wind energy conversion system (WECS). The station uses adaptive back stepping with the capacity to reject DC offsets. This study's main goals are listed in the following order.

The primary focus involves the aim of an integrated system that incorporates a PV array and WECS. This multifunctional system is tailored for Electric Vehicle (EV) charging and household power supply.

This study primarily focusses on the AFF-SOGI-DRC algorithm, which is responsible for controlling the charging station. Among its many potential uses is improving the grid's power quality in the face of dc offset in load currents and distorted or imbalanced voltages.

The charging station, PV array, and WECS are connected via a straightforward design. A rectifier and boost converter based topology is chosen when the PMSM has been found. Additionally, because the PV array is mechanically integrated into the charging station, a boost converter is not needed. All things considered, charging stations with a switchable between islanded and grid-connected modes are more efficient. The four quadrant operations enabled by the unified controller are vehicle-to-home power transfer, reactive power compensation, V2G/G2V power transfer, and active filtering. This charging station's adaptability is demonstrated by how easy it is to switch between grid-connected and island modes. This flexibility makes continuous charging possible, even in the event of grid outages, disruptions from wind and solar power, and overall system performance.

2. System Configuration And Control Algorithm

Voltage Source Converters(VSCs) are used by the integrated charging station that is shown in Figure1 to create connections between the PV array and WECS. Both Islanded Mode (IM) and Grid-Connected Mode (GCM) power supply to residential loads and electric vehicle (EV) charging are made easier by this combination. The direct current (dc) link of the charging station is specifically connected to the PV array. In contrast, a diodde bridge rectifier and a boost converter are used to connect the generator based Permanent Magnet Brushless DC (PMBLDC),Wind Energy Conversion System (WECS) to the dc link.

Boost converters are essential components of integrated charging stations because they optimise and capture the peak power produced by wind energy conversion systems (WECS). Efficient power extraction from the Point of Common Coupling (PCC) and the charging station's DC link is utilised by the electric vehicle (EV) in this coordinated system. A bidirectional dc–dc converter (BiDC) makes this bidirectional power flow possible. At the PCC of the entire system, the domestic loads are concurrently integrated effortlessly.

An interfacing inductors and a bidirectional static switch are added strategically to guarantee a suitable interface between the grid, the PCC, and the charging station. By efficiently eliminating switching harmonics, RC filters help to preserve the integrity of the power supply and reduce interference.

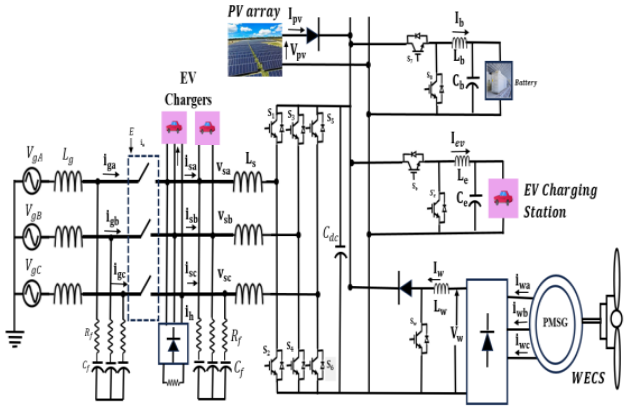

Fig1. Charging Station featuring renewable energy sources and electric chargers

The primary goal of the charging station can be summarized in two key objectives: to provide uninterrupted charging services to EVs under diverse operating conditions and to act as a reliable backup power source for household loads during emergencies. Consequently,In both Islanded Mode (IM) and Grid-Connected Mode (GCM), the charging station's control system is carefully designed to provide these vital services. Along with its main functions, the controller is very skilled at maximising power extraction from renewable sources, which is in line with the charging station's dedication to sustainability. Control techniques for GCM, IM, Maximum Power Point Tracking (MPPT) of the WECS, and a scheme for charging the storage battery are all part of the control system's complicated design to cater to the unique objectives of the charging station.

A. Control Strategy

To improve the system's power quality, the 6-pulse converter is controlled using the Adaptive Back Propagation (ABP) Algorithm. Its goal, as shown in Figure 2, is to separate the load currents across all phases into their component real and imaginary powers.

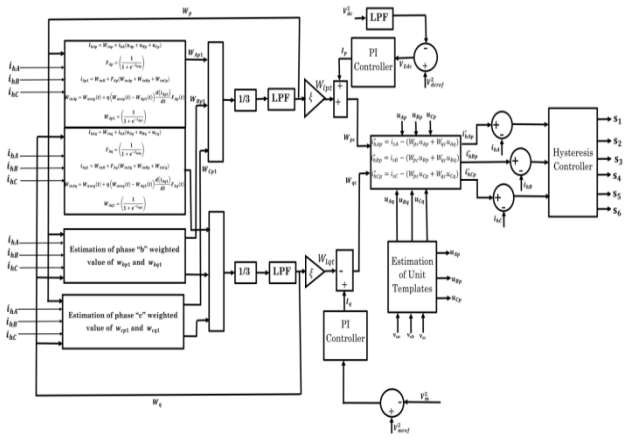

Fig2. Adaptive backstepping control with Hysteresis controller

1) Grid connected control using Adaptive Learning Back Propagation

The magnitude of the voltage (V_m) at PCC point is calculated as

$$V_m = \sqrt{\frac{2}{3} \times (V_{sA}^2 + V_{sB}^2 + V_{sC}^2)} \quad (1)$$

The estimation of in-phase normalized signals of grid voltages is calculated as follows:

$$u_{Ap} = \frac{V_{sA}}{V_m} \quad (2)$$

$$u_{Bp} = \frac{V_{sB}}{V_m} \quad (3)$$

$$u_{Cp} = \frac{V_{sC}}{V_m} \quad (4)$$

The grid's phase voltage, represented as V_{sA}, V_{sB}, and V_{sC} are used to estimate the quadrature normalized signals of grid voltages, following these steps.

$$u_{Aq} = \frac{-u_{Bp} + u_{Cp}}{\sqrt{3}} \quad (5)$$

$$u_{bq} = \frac{3u_{Ap} + u_{Bp} - u_{Cp}}{2\sqrt{3}} \quad (6)$$

$$u_{Cq} = \frac{-3u_{Ap} + u_{Bp} - u_{Cp}}{2\sqrt{3}} \quad (7)$$

The Adaptive back Propagation (ABP) control algorithm [25] calculates the weights for active components (W_{Ap}, W_{Bp}, W_{Cp}) and reactive components (W_{Aq}, W_{Bq}, W_{Cq}) of load currents. i_{ha}, i_{hb}, i_{hc} are non-linear load currents and their sampling interval serve as input variables for the controller. The ABP control algorithm's front-end layer is responsible for estimating the fundamental component of load current using equations.

$$I_{hAp} = W_{inp} + i_{hA}(u_{Ap} + u_{Bp} + u_{Cp}) \quad (8)$$

$$I_{hBp} = W_{inp} + i_{hB}(u_{Ap} + u_{Bp} + u_{Cp}) \quad (9)$$

$$I_{hCp} = W_{inp} + i_{hC}(u_{Ap} + u_{Bp} + u_{Cp}) \quad (10)$$

Here, W_{inp} symbolises the starting weight. Equations (7) to (9), which process the basic constituents of load currents,, and, using a sigmoid-type activation function. The feed-forward block's outputs are estimated using these formulas.

$$F_{Ap} = \left(\frac{1}{1 + e^{-i_{hAp}}}\right) \quad (11)$$

$$F_{Bp} = \left(\frac{1}{1 + e^{-i_{hBp}}}\right) \quad (12)$$

$$F_{Cp} = \left(\frac{1}{1 + e^{-i_{hCp}}}\right) \quad (13)$$

Feed forward block output are the inputs to a hidden layer in the backpropagation neural network. The outputs of the hidden layer are determined using equations (10) to (12).

$$i_{Ap1} = W_{inH} + F_{Ap}(W_{inAp} + W_{inBp} + W_{inCp}) \quad (14)$$

$$i_{Bp1} = W_{inH} + F_{Bp}(W_{inAp} + W_{inBp} + W_{inCp}) \quad (15)$$

$$i_{Cp1} = W_{inH} + F_{Cp}(W_{inAp} + W_{inBp} + W_{inCp}) \quad (16)$$

$W_{inAp}, W_{inBp}, W_{inCp}$ and W_{inH} are initial weights of the hidden layer which are calculated using following equations

$$W_{inAp} = W_{avep}(t) + \eta\left(W_{avep}(t) - W_{Ap1}(t)\right)\frac{d(i_{Ap1})}{dt}F_{Ap}(t) \quad (17)$$

$$W_{inBp} = W_{avep}(t) + \eta\left(W_{avep}(t) - W_{Bp1}(t)\right)\frac{d(i_{Bp1})}{dt}F_{Bp}(t) \quad (18)$$

$$W_{inCp} = W_{avep}(t) + \eta\left(W_{avep}(t) - W_{Cp1}(t)\right)\frac{d(i_{Cp1})}{dt}F_{Cp}(t) \quad (19)$$

In this scenario, $W_{avep}(t)$ means that the active power component of load currents has an average weight, while $W_{inAp}(t), W_{inBp}(t), W_{inCp}(t)$ reflects the revised beginning weight value at the t^{th} sampling time for phases A, B, and C, respectively. $W_{Ap1}(t), W_{Bp1}(t), W_{Cp1}(t)$ denote the amplitudes of the fundamental weight of the active power component of load currents for phase A, B and C respectively. $F_{Ap}(t), F_{Bp}(t)$ and $F_{Cp}(t)$ denote the output of the feed-forward blocks. η denotes the learning rate of the neural network.

Sigmoid function is used as the activation function for the neural network and calculated the values of the fundamental real power components $W_{Ap1}(t), W_{Bp1}(t)$ and $W_{Cp1}(t)$.

The calculated values of i_{Rp1}, i_{Yp1}, and i_{Bp1} undergo processing through a sigmoid function, which acts as the activation function of the neural network. This process aims to estimate the fundamental real power components of load currents (W_{Rp1}, W_{Yp1}, W_{Bp1}).

$$W_{Ap1} = \left(\frac{1}{1 + e^{-i_{Ap1}}}\right) \quad (20)$$

$$W_{Bp1} = \left(\frac{1}{1 + e^{-i_{Bp1}}}\right) \quad (21)$$

$$W_{Cp1} = \left(\frac{1}{1 + e^{-i_{Cp1}}}\right) \quad (22)$$

The average weight of the fundamental real power signal (W_p) is determined as follows.

$$W_p = \frac{W_{Ap} + W_{Bp} + W_{Cp}}{3} \quad (23)$$

W_{lpt} is the weight of the active power component which can be calculated by multiplying W_p with a scaling factor ξ after filtering higher frequency ripples with lowpass filter.

Similarly weight of the reactive power component W_{lqt} can be calculated using following equations.

$$I_{hAq} = W_{inq} + i_{hA}(u_{Aq} + u_{Bq} + u_{Cq}) \quad (24)$$

$$I_{hBq} = W_{inq} + i_{hB}(u_{Aq} + u_{Bq} + u_{Cq}) \quad (25)$$

$$I_{hCq} = W_{inq} + i_{hC}(u_{Aq} + u_{Bq} + u_{Cq}) \quad (26)$$

$$F_{Aq} = \left(\frac{1}{1 + e^{-i_{hAq}}}\right) \quad (27)$$

$$F_{Bq} = \left(\frac{1}{1 + e^{-i_{hBq}}}\right) \quad (28)$$

$$F_{Cq} = \left(\frac{1}{1 + e^{-i_{hCq}}}\right) \quad (29)$$

$$i_{Aq1} = W_{inH} + F_{Aq}(W_{inAq} + W_{inBq} + W_{incq}) \quad (30)$$

$$i_{Bq1} = W_{inH} + F_{Bq}(W_{inAq} + W_{inBq} + W_{incq}) \quad (31)$$

$$i_{Cq1} = W_{inH} + F_{Cq}(W_{inAq} + W_{inBq} + W_{incq}) \quad (32)$$

$$W_{inAq} = W_{aveq}(t) + \eta\left(W_{aveq}(t) - W_{Aq1}(t)\right)\frac{d(i_{Aq1})}{dt}F_{Aq}(t) \quad (33)$$

$$W_{inBq} = W_{aveq}(t) + \eta\left(W_{aveq}(t) - W_{Bq1}(t)\right)\frac{d(i_{Bq1})}{dt}F_{Bq}(t) \quad (34)$$

$$W_{incq} = W_{aveq}(t) + \eta\left(W_{aveq}(t) - W_{Cq1}(t)\right)\frac{d(i_{Cq1})}{dt}F_{Cq}(t) \quad (35)$$

$$W_{Aq1} = \left(\frac{1}{1 + e^{-i_{Aq1}}}\right) \quad (36)$$

$$W_{Bq1} = \left(\frac{1}{1 + e^{-i_{Bq1}}}\right) \quad (37)$$

$$W_{Cq1} = \left(\frac{1}{1 + e^{-i_{Cq1}}}\right) \quad (38)$$

$$W_q = \frac{W_{Aq} + W_{Bq} + W_{Cq}}{3} \quad (39)$$

W_{lqt} is the weight of the reactive power component which can be calculated by multiplying W_q with a scaling factor α after filtering higher frequency ripples with lowpass filter.

DC voltage across the capacitor C_{dc} can be regulated by using a PI controller. Input of the PI controller is error between square of the reference and actual DC voltage. And output of the controller is given as

$$I_p(t) = I_p(t-1) + K_{i1}\big(V_{Edc}(t) - V_{Edc}(t-1)\big) + K_{p1}\big(V_{Edc}(t)\big) \quad (40)$$

Where $V_{Edc}(t) = V_{dcref}^2(t) - V_{dc}^2(t)$.Then voltage magnitude at PCC can be regulated by another PI controller and output is given as

$$I_q(t) = I_q(t-1) + K_{i2}\big(V_{Em}(t) - V_{Em}(t-1)\big) + K_{p2}\big(V_{Em}(t)\big) \quad (41)$$

Where $V_{mdc}(t) = V_{mref}^2(t) - V_m^2(t)$.Active and reactive power magnitudes (W_{pc} and W_{qc}) which constitute for reference currents are calculated by using weights of the active and reactive power components.

$$W_{pc} = I_p(t) + W_{lpt} \quad (42)$$

$$W_{qc} = I_q(t) - W_{lqt} \quad (43)$$

Then reference currents are calculated using

$$i_{hAp}^* = i_{sA} - \big(W_{pc}u_{Ap} + W_{qc}u_{Aq}\big) \quad (44)$$

$$i_{hBp}^* = i_{sB} - \big(W_{pc}u_{Bp} + W_{qc}u_{Bq}\big) \quad (45)$$

$$i_{hCp}^* = i_{sC} - \big(W_{pc}u_{Cp} + W_{qc}u_{Cq}\big) \quad (46)$$

The net reference currents (i_{hAp}^*, i_{hBp}^* and i_{hCp}^*) are compared with the sensed currents (i_{hAp}, i_{hBp} and i_{hCp}), and the error for each phase current is processed through the hysteresis PWM controller. This process generates the gating pulses (S_1, S_2, S_3, S_4, S_5 and S_6) for the corresponding leg of the Voltage Source Converter (VSC).

2) Islanding mode control

Wind energy conversion systems (WECS) and photovoltaic (PV) array power are intended to be used with the islanding mode control. During blackouts in the grid, it runs the charging station. Fig. 2 illustrates the control method that generates AC voltages at the point of common coupling (PCC). An oscillating reference voltage is produced by this control. In order to create current references for PCC, the control system compares these reference voltages with measured voltages and uses PI regulators to minimise voltage mistakes. The smooth transition between grid-connected and islanding modes is another concern of the islanding mode control system. To identify the operating mode, the controller measures the phase error between the grid and Point of Common Coupling (PCC) voltages continually. Initial phase error assessment occurs during transitioning. Reducing the phase error in terms of frequency error is the goal of a proportional-integral (PI) controller. During this transition phase, the frequency error is computed.

$$\omega(t) = \omega(t-1) + K_{i3}\big(\theta_e(t) - \theta_e(t-1)\big) + K_{p3}\theta_e(t) \quad (47)$$

Where $\theta_e = \theta_{grid} - \theta_{pcc}$

Then the frequency can be updated as

$$\omega_t = \omega_r + \omega \quad (48)$$

If the phase error doesn't match the conditions in Fig. 2, the converter will update the frequency voltage. The controller initiates the signal, which allows the Point of Common Coupling (PCC) to be connected to the grid, if all the prescribed conditions are satisfied.

3) Bidirectional Converter Control for Storage Battery

In the G2S mode of the grid connected mode, the battery operates usinga method based on constantly available current and voltage, on the other hand, in the S2G mode, the battery undergoes discharge with a constant current/power approach. The specific current/power value is contingent on the charging station's commitment to the utility.Fig3. shows the Bidirectional Converter for battery using PI controller

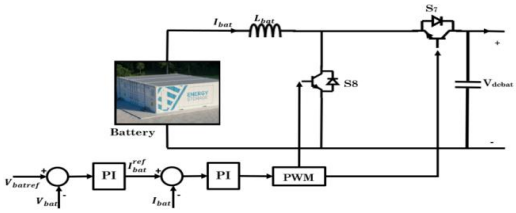

Fig3. Bidirectional Converter for battery

4) *Power Generation System Using Wind*

The Maximum Power Point Tracking (MPPT) Control Wind Energy Conversion System (WECS) is illustrated in Figure 4 as a schematic.In order to accomplish maximum power point tracking (MPPT), an Incremental Conductance (INC) MPPT method is used with the current and voltage output from the rectifier to estimate the voltage that corresponds to the maximum power. The Pulse Width Modulation (PWM) generator then uses the Maximum Power Point (MPP) voltage and the dc-link voltage to generate the triggering signals for a boost converter.

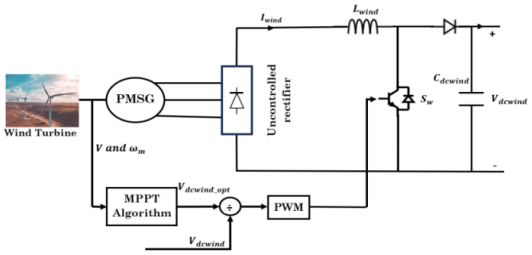

Fig4. Wind generating station with DC-DC Converter.

B. RESULTS AND DISCUSSION

Simulation of the charging station with proposed adaptive learning back propagation is developed in MATLAB/SIMULINK.Figures 5–9 provide examples of the system's operational capability in both dynamic and steady-state scenarios.The charging station can operate in grid or islanding mode; both modes exhibit dynamic performances. For simulation, a 2.5 kW, 460 V, and 9.5 A solar PV array is utilized, and wind generation system rating is 2kW. The battery is rated at 240 V and 35 Ah. Table I provides the system's detailed parameters..

Table. 1. Parameters of the system

Parameter	Value/Rating
PV array	4.37kW
Open circuit Voltage (Voc)	52V
Short Circuit Current (Isc)	5.15A
Voltage at Maximum Power Point Vmp(V)	46V
Current at Maximum Power Point Imp	4.75A
Parallel strings	2
Series-connected modules per string	10
Battery rating	240V, 35Ah
Grid	230V, 50Hz
PMSG rating	2kW
DC Link Capacitor	1000µF
Load	20Ω, 10mH

1) Steady State Response

In Fig. 5, we can see how well the constructed charging station performs under steady-state settings while linked to the grid. Combined, the voltage and current in Fig. 5(a), load Fig. 5(b), and voltage and current in VSC Fig. 5(c). Figure 5(d) shows the grid current's Total Harmonic Distortion (THD). Grid current displays a total harmonic distortion(THD) of less than 5%, despite the fact that electric vehicle (EV) current drawn at the Point of Common Coupling (PCC) surpasses 20%. The charging station's resilience and adaptability in Grid-to-Charging Mode are highlighted by the comprehensive results shown in Figure 5 and Table II.

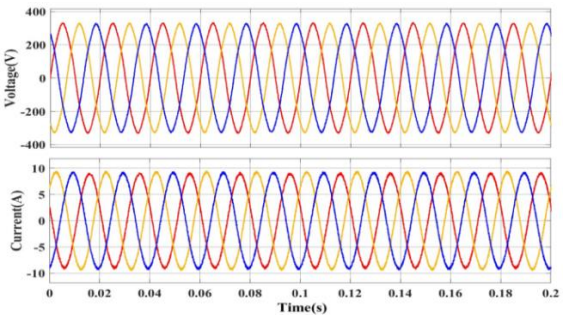

(a)

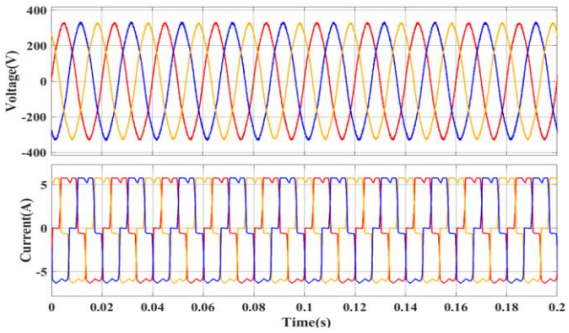

(b)

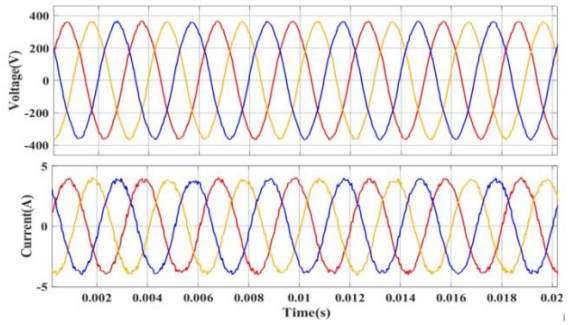

(c)

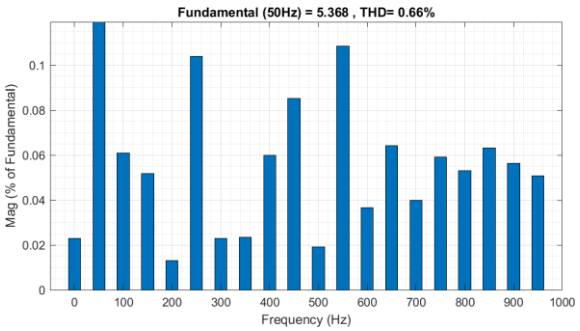

(d)

Fig5. (a) Grid Voltage and current, (b) Load voltage and current,

(c) VSC voltage and current (d) Grid current THD

Table.2 Comparison of THD

Parameter	AFF-SOGI-DRC [20]	Proposed Adaptive Backstepping Control
Grid Current		
I_{gA}	4.4%	0.66%
I_{gB}	3.9%	0.68%
I_{gC}	4.21%	0.68%
Grid Voltage		
V_{gA}	2.4%	0.89%
V_{gB}	2.36%	0.82%
	2.45%	0.83%

V_{gC}		
Load Current		
I_{hA}	25.94%	25.94%
I_{hB}	25.95%	25.95%
I_{hC}	25.95%	25.95%
Load Voltage		
V_{hA}	2.9%	0.78%
V_{hB}	2.94%	0.72%
V_{hC}	2.83%	0.72%

2) *Dynamic Response*

As the solar irradiation drops from 1000 to 500 W/m2, the current flowing through the PV array drops as well. The electric car and the Wind Energy Conversion System (WECS) are connected at the Point of Common Coupling (PCC), so the battery is discharged to maintain control over their power levels.

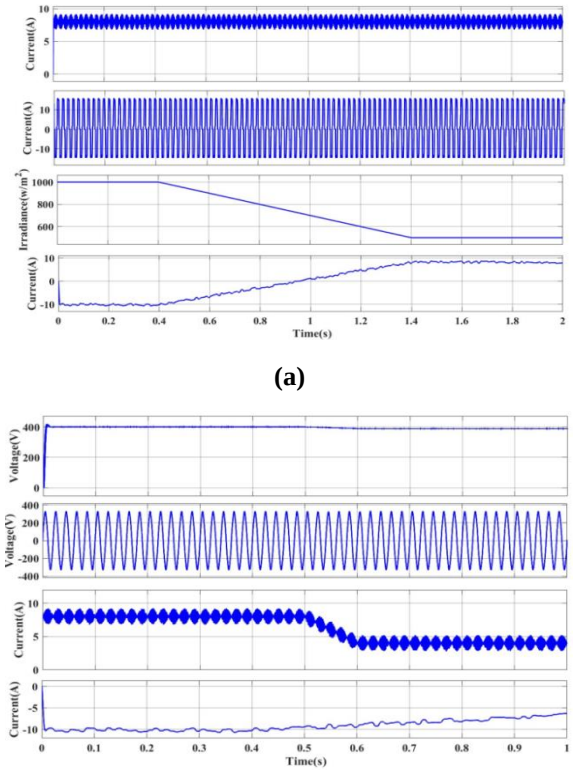

(a)

(b)

Fig6. (a) wind current (I_w), Load current in phase A (I_{sA}), Irradiance (G) and battery current (I_b) during change in Irradiance (b) DC link Voltage (V_{dc}), VSC voltage in Phase A (V_{sA}), wind current (I_w), and battery current (I_b) during change in wind speed in islanding mode

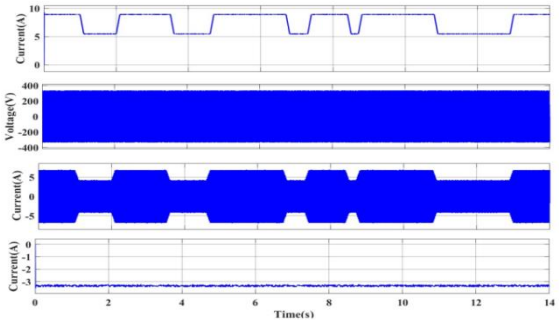

(a)

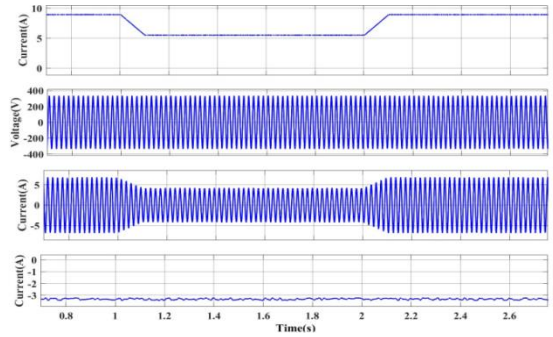

(b)

Fig7. (a) PV current (P_{pv}), grid voltage in phase A (V_{gA}), grid current in phase A (I_{gA}), battery current (I_b) during irradiance change and grid connected mode (b) zoomed waveforms

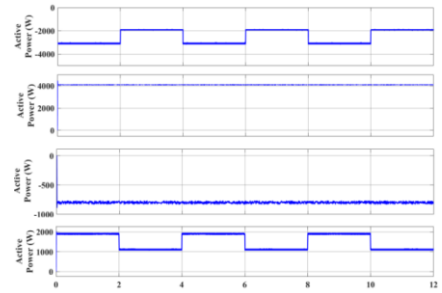

(a)

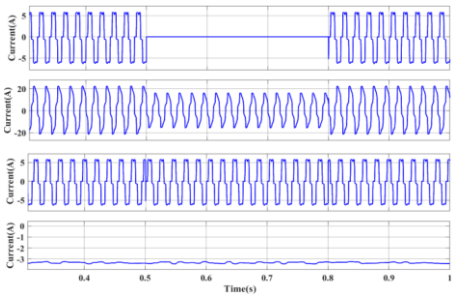

(b)

Fig8. (a) Grid power (P_g), PV power (P_{pv}), battery power (P_b) and wind power (P_w) during wind speed change and grid connected mode (b) load current in phase A (I_{hA}), load current in phase B (I_{hB}), load current in phase C (I_{gC}) and battery current (I_b)

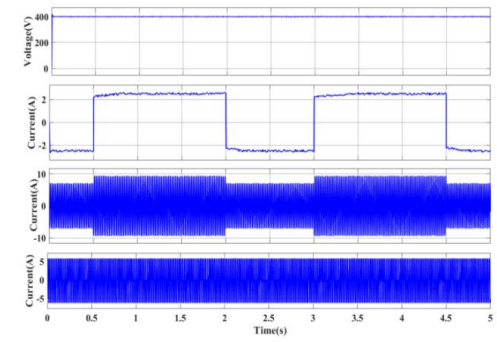

(a)

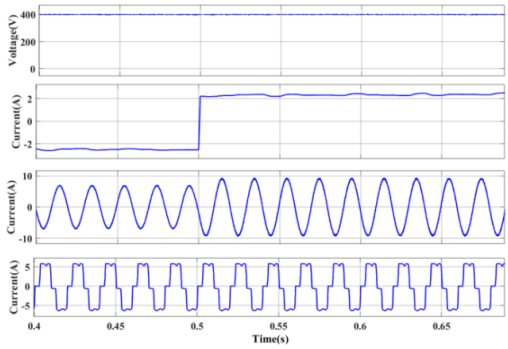

(b)

Fig9. (a) DC link Voltage (V_{dc}), battery current (I_b), grid current in phase A and load current (I_{hA}) during change in I_b in grid connected mode (b) zoomed waveforms during increase in I_b

2) Increased generation

To assess the effectiveness of the proposed Adaptive Backstepping Control algorithm in enhancing power quality at a renewable energy-based grid-connected EV charging station, the generation capacities of both wind and PV sources are boosted. Consequently, the load is also increased to adequately accommodate the improved generation capacities. The wind generation capacity is boosted from 2 kW to 3.75kW, while the PV generation capacity is raised from 4.3 kW to 5.2kW. Additionally, the number of series-connected modules per string is increased from 10 to 12 to attain the necessary generation capacity from the PV system. Updated parameters of the system are given in table III.

Table. 3. Updated PARAMETERS OF THE SYSTEM FOR increased generation

Parameter	Value
PV array	5.2kW
Open Circuit Voltage Voc(V)	52V
Short Circuit Current Isc (A)	5.15A
Voltage at Maximum Power Point Vmp(V)	46V
Current at Maximum Power Point Imp (A)	4.75A
Parallel strings	2
Series-connected modules per string	12
Battery rating	240V, 50Ah
Grid	230V, 50Hz
PMSG rating	3.75kW
DC Link Capacitor	1000µF
Load	25Ω, 10mH

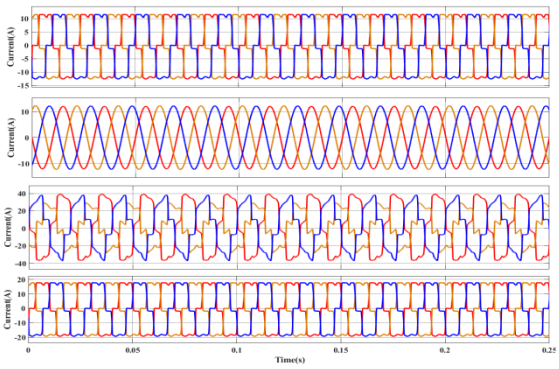

Fig10. (a) Non-Linear load current (b) Grid Current (c) VSI Current (d) EV Charging Current

In Fig10.Shows the nonlinear load currents,Grid Currents. Voltage Source Inverter Current and EV Charging Current with increased Generation of solar,wind.

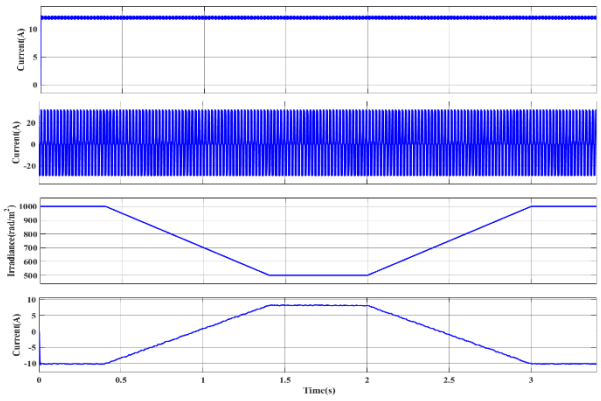

Fig 11.wind current(I_w),Load current in phaseA (I_{sA}),(c) VSI Current (d) EV Charging Current Irradiance and battery current (I_b) during change in Irradiance

The Fig11. Indicated the change in irradiance the battery will gives the supply to maintain load current constant

3. Conclusion

This paper presented the application of Adaptive Backstepping Control in the context of a Renewable Energy-Based GICS for EVs, focused on enhancing power

quality during the electrical vehicle charging process. The Adaptive Backstepping Control algorithm is designed to adapt to the dynamic and uncertain nature of renewable energy inputs, providing a robust and efficient control framework for the GICS. By optimizing the power flow and addressing fluctuations in renewable energy generation, the system aims to improve power quality metrics such as voltage regulation and harmonic mitigation during the EV charging operation. In order to assess how effective the suggested Adaptive Backstepping Control, a comparative analysis is conducted against the Adaptive Frequency-Fixed Second Order Generalized Integrator with DC offset rejection capability, which represents a state-of-the-art control approach. The comparison encompasses key performance indicators, including power quality indices, transient response, and overall system stability. The results of the two methods are compared and concluded that the Adaptive Backstepping Control method provides the best power quality in the proposed system with reduction of harmonics.

References

[1] Aguero, J.R.; Takayesu, E.; Novosel, D.; Masiello, R. Modernizing the Grid: Challenges and Opportunities for a Sustainable Future. IEEE Power Energy Mag. 2017, 15, 74–83.

[2] Naqvi, S.B.Q.; Kumar, S.; Singh, B. Weak Grid Integration of a Single-Stage Solar Energy Conversion System With Power Quality Improvement Features Under Varied Operating Conditions. IEEE Trans. Ind. Appl. 2021, 57, 1303–1313.

[3] Kwon, M.; Park, S.; Oh, C.-Y.; Lee, J.; Choi, S. Unified Control Scheme of Grid-Connected Inverters for Autonomous and Smooth Transfer to Stand-Alone Mode. IEEE Trans. Power Electron. 2022, 37, 416–425.

[4] Aguero, J.R.; Takayesu, E.; Novosel, D.; Masiello, R. Modernizing the Grid: Challenges and Opportunities for a Sustainable Future. IEEE Power Energy Mag. 2017, 15, 74–83.

[5] Naqvi, S.B.Q.; Kumar, S.; Singh, B. Weak Grid Integration of a Single-Stage Solar Energy Conversion System With Power Quality Improvement Features Under Varied Operating Conditions. IEEE Trans. Ind. Appl. 2021, 57, 1303–1313.

[6] Kwon, M.; Park, S.; Oh, C.-Y.; Lee, J.; Choi, S. Unified Control Scheme of Grid-Connected Inverters for Autonomous and Smooth Transfer to Stand-Alone Mode. IEEE Trans. Power Electron. 2022, 37, 416–425.

[7] Chan, C.C. The State of the Art of Electric, Hybrid, and Fuel Cell Vehicles. Proc. IEEE 2007, 95, 704–718.

[8] Su,W.; Eichi, H.; Zeng,W.; Chow, M.-Y. A Survey on the Electrification of Transportation in a Smart Grid Environment. IEEE Trans. Ind. Inform. 2012, 8, 1–10.

[9] Chan, C.C.; Bouscayrol, A.; Chen, K. Electric, Hybrid, and Fuel-Cell Vehicles: Architectures and Modeling. IEEE Trans. Veh. Technol. 2010, 59, 589–598.

[10] Lopes, J.A.P.; Soares, F.; Almeida, P.M.R. Integration of Electric Vehicles in the Electric Power Systems. Proc. IEEE 2011, 99, 168–183.

[11] Chan, C.C. The State of the Art of Electric, Hybrid, and Fuel Cell Vehicles. Proc. IEEE 2007, 95, 704–718.

[12] Lopes, J.A.P.; Soares, F.; Almeida, P.M.R. Integration of Electric Vehicles in the Electric Power Systems. Proc. IEEE 2011, 99, 168–183.

[13] Carlos Gómez, J.; Morcos, M.M. Impact of EV Battery Chargers on the Power Quality of Distribution Systems. IEEE Trans. Power Del. 2003, 18, 975–981.

[14] Paterakis, N.; Erdinc, O.; Bakirtzis, A.G.; Catalão, J.P.S. Optimal Household Appliances Scheduling Under Day-Ahead Pricing and Load-Shaping Demand Response Strategies. IEEE Trans. Ind. Inform. 2015, 11, 1509–1519.

[15] Chen, C.; Duan, S. Optimal Integration of Plug-In Hybrid Electric Vehicles in Microgrids. IEEE Trans. Ind. Inform. 2014, 10, 1917–1926.

[16] Gungor, V.C.; Sahin, D.; Kocak, T.; Ergut, S.; Buccella, C.; Cecati, C.; Hancke, G. Smart Grid and Smart Homes: Key Players and Pilot Projects. IEEE Ind. Electron. Mag. 2012, 6, 18–34.

[17] Monteiro, V.; Monteiro, L.F.C.; Franco, F.L.; Mandrioli, R.; Ricco, M.; Grandi, G.; Afonso, J.L. The Role of Front-End AC/DC Converters in Hybrid AC/DC Smart Homes: Analysis and Experimental Validation. Electronics 2021, 10, 2061.

[18] Arif, S.M.; Lie, T.T.; Seet, B.C.; Ayyadi, S.; Jensen, K. Review of Electric Vehicle Technologies, Charging Methods, Standards and Optimization Techniques. Electronics 2021, 10, 1910.

[19] Afonso, J.L.; Cardoso, L.A.L.; Pedrosa, D.; Sousa, T.J.C.; Machado, L.; Tanta, M.; Monteiro, V. A Review on Power Electronics Technologies for Electric Mobility. Energies 2020, 13, 6343.

[20] Teng, F.; Ding, Z.; Hu, Z.; Sarikprueck, P. Technical Review on Advanced Approaches for Electric Vehicle Charging Demand Management, Part I: Applications in Electric Power Market and Renewable Energy Integration. IEEE Trans. Ind. Appl. 2020, 56, 5684–5694.

[21] Ding, Z.; Teng, F.; Sarikprueck, P.; Hu, Z. Technical Review on Advanced Approaches for Electric Vehicle Charging Demand Management, Part II: Applications in Transportation System Coordination and Infrastructure Planning. IEEE Trans. Ind. Appl. 2020, 56, 5695–5703.

[22] Zeng, M.; Leng, S.; Zhang, Y. Power charging and discharging scheduling for V2G networks in the smart grid. In Proceedings of the 2013 IEEE International Conference on CommunicationsWorkshops (ICC), Budapest, Hungary, 9–13 June 2013; pp. 1052–1056. Electronics 2022, 11, 429 19 of 19

[23] Yu, R.; Zhong, W.; Xie, S.; Yuen, C.; Gjessing, S.; Zhang, Y. Balancing Power Demand through EV Mobility in Vehicle-to-Grid Mobile Energy Networks. IEEE Trans. Ind. Informat. 2016, 12, 79–90.

[24] Verma, Anjeet, and Bhim Singh. "AFF-SOGI-DRC control of renewable energy based grid interactive charging station for EV with power quality improvement." IEEE Transactions on Industry Applications 57.1 (2020): 588-597.

[25] Kalla, Ujjwal Kumar, et al. "Adaptive control of voltage source converter based scheme for power quality improved grid-interactive solar PV–battery system." IEEE Transactions on Industry Applications 56.1 (2019): 787-799.